JACS
JOURNAL OF THE AMERICAN CHEMICAL SOCIETY

Article

pubs.acs.org/JACS

Reversibly Switching Bilayer Permeability and Release Modules of Photochromic Polymersomes Stabilized by Cooperative Noncovalent Interactions

Xiaorui Wang,[†] Jinming Hu,[†] Guhuan Liu,[†] Jie Tian,[‡] Huijuan Wang,[‡] Ming Gong,[‡] and Shiyong Liu*[,†]

[†]CAS Key Laboratory of Soft Matter Chemistry, Hefei National Laboratory for Physical Sciences at the Microscale, iChem (Collaborative Innovation Center of Chemistry for Energy Materials), Department of Polymer Science and Engineering, University of Science and Technology of China, Hefei, Anhui 230026, China

[‡]Engineering and Materials Science Experiment Center, University of Science and Technology of China, Hefei, Anhui 230027, China

Supporting Information

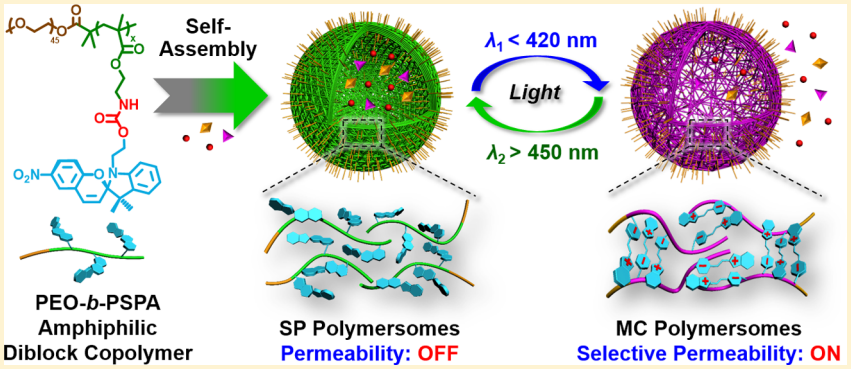

ABSTRACT: We report on the fabrication of photochromic polymersomes exhibiting photoswitchable and reversible bilayer permeability from newly designed poly(ethylene oxide)-*b*-PSPA (PEO-*b*-PSPA) diblock copolymers, where SPA is spiropyran (SP)-based monomer containing a unique carbamate linkage. Upon self-assembling into polymersomes, SP moieties within vesicle bilayers undergo reversible phototriggered isomerization between hydrophobic spiropyran (SP, λ_2 > 450 nm irradiation) and zwitterionic merocyanine (MC, λ_1 < 420 nm irradiation) states. For both SP and MC polymersomes, their microstructures are stabilized by multiple cooperative noncovalent interactions including hydrophobic, hydrogen bonding, $\pi-\pi$ stacking, and paired electrostatic (zwitterionic) interactions, with the latter two types being exclusive for MC polymersomes. Control experiments using analogous block copolymers of hydrophobic SP monomer with a carbonate linkage (SPO) and conventional spiropyran methacrylate monomer (SPMA) containing a single ester functionality were then conducted, revealing that carbamate-incurred hydrogen bonding interactions in PEO-*b*-PSPA are crucial for polymersome stabilization in the zwitterionic MC state. Moreover, reversible phototriggered SP-to-MC polymersome transition is accompanied by membrane polarity and permeability switching from being nonimpermeable to selectively permeable toward noncharged, charged, and zwitterionic small molecule species below critical molar masses. Intriguingly, UV-actuated MC polymersomes possess two types of release modules: (1) sustained release upon short UV irradiation duration by taking advantage of the unexpectedly slow spontaneous MC-to-SP transition kinetics ($t_{1/2}$ > 20 h) under dark conditions; (2) on-demand and switchable release under alternated UV−vis light irradiation. We further demonstrate photoswitchable spatiotemporal release of 4′,6-diamidino-2-phenylindole (DAPI, cell nuclei-staining dye) within living HeLa cells.

INTRODUCTION

In living organisms, cellular structures and organelles are highly compartmentalized and spatially segregated by phospholipid-based membranes, and normal cellular functions rely on efficient and selective extra/intracellular communications. Although phospholipid bilayer membranes exhibit limited permeability for biomolecules, ions, and water molecules due to the hydrophobic nature, various substrate-selective membrane channel proteins are integrated with cellular membranes to facilitate mass transport with excellent precision and specificity.[1] Long-standing efforts of mimicking intricate structures and functions of cellular components have continuously spurred the creation of a variety of self-assembled nanostructures.[2] Among them, lipid vesicles (liposomes) and amphiphilic block copolymer (BCP) vesicles (polymersomes) stand for two representative prototypes, both consisting of aqueous interiors enclosed by hydrophobic bilayer mem-

Received: September 26, 2015
Published: November 19, 2015

DOI: 10.1021/jacs.5b10127
J. Am. Chem. Soc. 2015, 137, 15262−15275

Scheme 1. Photochromic Polymersomes Exhibiting Photoswitchable and Reversible Bilayer Permeability[a]

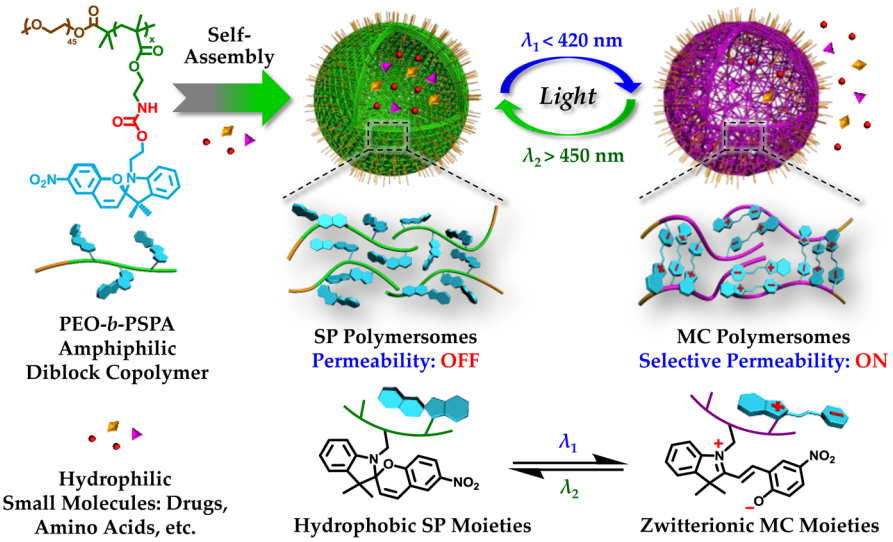

[a]Amphiphilic PEO-*b*-PSPA diblock copolymers self-assemble into polymersomes with hydrophobic bilayers containing carbamate-based hydrogen-bonding motifs. Spiropyran moieties within polymersome bilayers undergo reversible photo-triggered isomerization between hydrophobic spiropyran (SP, λ_2 > 450 nm irradiation) and zwitterionic merocyanine (MC, λ_1 < 420 nm irradiation) states. The microstructures of both SP and MC polymersomes are synergistically stabilized due to cooperative noncovalent interactions from hydrophobic, hydrogen bonding, $\pi-\pi$ stacking, and paired electrostatic (zwitterionic) interactions, with the latter two types being exclusive for MC polymersomes. Moreover, reversible photo-triggered SP/MC polymersome transition is accompanied with membrane permeability switching from being non-impermeable to selectively permeable towards non-charged, charged, and zwitterionic small molecule species below critical molar masses.

branes.[3] Compared to liposomes, polymersomes possess distinct advantages including improved structural stability, tunable architectural parameters, and facile functional integration. Thus, they have been increasingly utilized to construct drug delivery nanocarriers,[4] nanoreactors,[5] and artificial organelles.[6]

However, conventional polymersomes are subjected to severe membrane permeability issues due to the hydrophobicity and macromolecular nature of thick bilayers, which are almost impermeable to small molecules, ions, and even water molecules.[7] This poses considerable impediments toward the further exploration of relevant functions. To solve this challenge, a number of approaches have been invented to enhance permeability such as physical/chemical integration of natural channel proteins and stimuli-responsive moieties into polymersome bilayers,[8] and in situ postmodification reactions within bilayer membranes.[9] However, these approaches either involve complex fabrication procedures or require the introduction of external additives, leading to inadequate extent of process control and compromised permselectivity. Most importantly, these permeability-enhancing processes are usually irreversible and might be accompanied by the loss of structural integrity or even complete disintegration of polymersome structures. Thus, the screening of novel strategies for facile, switchable, and reversible regulation of polymersome bilayer permeability with predicted precision while maintaining the microstructural stability remains a considerable challenge.

Among those conventionally applied stimuli to regulate polymersome permeability, light stimulus possesses distinctive advantages such as facile operation, spatiotemporal and wavelength-selective precision, no external additives, and feasibility of remote control within closed systems.[10] Recently, we proposed a new approach to solve the dilemma between structural stability and permeability switching of polymersomes by virtue of light-triggered "traceless" cross-linking of photo-responsive bilayers.[11] However, the process is irreversible and bilayer cross-linking is accompanied by unidirectional hydrophobicity-to-hydrophilicity transition; in addition, phototriggered release of small molecule reactive intermediates (e.g., 2-nitrosobenzaldehyde) might further incur cytotoxicity issues. Note that the reversible regulation of polymersome permeability enables not only the mimicking of cellular transport processes but also programmed payload release under pathologically relevant complex microenvironments. Albeit highly desirable, to the best of our knowledge, the reversible, off-on switchable, and spatiotemporal manipulation of polymersome permeability under "additive-free" conditions has been far less explored.

On the other hand, spiropyran (SP) is a well-known photochromic molecule that has been widely utilized in photoresponsive dynamic materials for optical/electrical switches,[12] drug nanocarriers,[13] self-erasing (reusable) paper,[14] and super-resolution imaging.[15] SP moieties can respond to light irradiation in a wavelength-selective manner and undergo reversible isomerization between colorless ring-closed SP state and colored ring-opened merocyanine (MC) state. Generally, under shorter wavelength irradiation (e.g., λ_1 < 420 nm), initially hydrophobic SP moieties transform into hydrophilic zwitterionic MC moieties, which is also accompanied by microenvironmental polarity switching.[16] Meanwhile, the SP-to-MC isomerization process can be readily reversed under longer wavelength irradiation (e.g., λ_2 > 450 nm).[17] On the basis of the light-tunable feature, we envisaged that if SP functionalities were incorporated into polymersome bilayers, the unique SP-to-MC photochromic transition might be exploited for reversibly regulating the permeability of polymersomes.

Nevertheless, previous studies revealed that phototriggered SP-to-MC transitions can render considerable shift in the hydrophobicity–hydrophilicity balance, leading to prominent

DOI: 10.1021/jacs.5b10127
J. Am. Chem. Soc. 2015, 137, 15262–15275

microstructural rearrangement and disintegration of nanoparticles self-assembled from amphiphilic block or random copolymers of SP-based methacrylate monomer containing a single ester linkage (SPMA).[13c,16a,c,18] Recently, Gong et al.[19] reported that random copolymerization of cationic and anionic monomers in aqueous media at high concentrations (>0.7−1.0 M) directly led to tough, viscoelastic, and self-healing single-component polymeric hydrogels. These results implied that paired ionic (i.e., zwitterionic) interactions are strong enough to stabilize microstructures if they possess a high local density. Note that paired electrostatic or zwitterionic interactions are closely relevant to light-actuated zwitterionic MC moieties, as implied by previous reports concerning the transport of amino acids aided by photoresponsive SP encapsulated within liposome bilayers.[20] For zwitterionic MC, $\pi-\pi$ stacking interactions between MC moieties are also prominent due to their coplanar nature. In this context, Vamvakaki et al.[21] reported that for UV-irradiated hybrid silica nanoparticles coated with SPMA-containing polymer brushes (~6.1 mol %), UV-actuated H-type $\pi-\pi$ stacking interactions between ring-opened MC species can stabilize and render nanocapsule formation upon etching off silica cores, whereas visible light irradiation at later stages led to nanocapsule disruption due to the loss of efficient $\pi-\pi$ stacking interactions upon restoring to the SP state.

The above reports prompted us to speculate whether we could take advantage of synergistic noncovalent interactions (i.e., zwitterionic interactions and $\pi-\pi$ stacking interactions) between ring-opened MC moieties to concurrently stabilize polymersome microstructures and reversibly switch bilayer permeability under alternate UV−vis light irradiation. After reasoning that the extent of MC-MC orientation within polymersome bilayers should play crucial roles in strengthening cooperative interactions, we attempted to start with a new SP-containing monomer incorporated with a carbamate linkage (SPA; Scheme S1a). We envisaged that carbamate-incurred hydrogen bonding interactions will lead to preorganization of SP moieties within bilayer membranes of polymersomes self-assembled from amphiphilic block copolymers of SPA; upon UV irradiation, enhanced cooperative MC-MC interactions will occur due to elevated degree of orientation between MC moieties (Scheme 1).

To testify this presumption, photochromic amphiphilic block copolymers (BCPs), poly(ethylene oxide)-*b*-PSPA (PEO-*b*-PSPA), were synthesized (Scheme S1a). They self-assembled in aqueous media into stable polymersomes consisting of aqueous lumens entrapped by hydrophobic PSPA bilayers with low permeability. Upon light irradiation with λ_1 < 420 nm, SP moieties transformed into hydrophilic zwitterionic MC derivatives. Most importantly, MC polymersomes were extremely stable due to cooperative noncovalent interactions including hydrophobic and hydrogen bonding interactions, and emerging zwitterionic and $\pi-\pi$ stacking interactions between preorganized MC residues. The photoisomerization process was accompanied by microenvironmental polarity and bilayer permeability switching. In addition, zwitterionic MC residues were subjected to ring closure into SP moieties under light irradiation with λ_2 > 450 nm, leading to the recovery of original SP polymersomes with switched-off permeability. Under alternate λ_1/λ_2 light irradiation, the above permeability switch on/off process could be repeated without disintegration of polymersome structures (Scheme 1). We then demonstrated photoswitchable intracellular delivery of hydrophilic small molecule substances in a spatiotemporal manner. To further verify the generality and validity of reversible membrane permeability, switchable fluorogenic reactions within fluorescent probe-encapsulated PEO-*b*-PSPA microcapsule reactors were achieved via light-regulated access of external amino acids and hydrated protons through microcapsule membranes.

RESULTS AND DISCUSSION

Synthesis and Self-Assembly of Photochromic Amphiphilic Diblock Copolymers. Previous reports concerning SP-containing amphiphilic block or random copolymers synthesized via controlled radical polymerizations exclusively utilized SP-based methacrylate monomer with only one ester functionality (SPMA, see Scheme S1c).[13c,16a,c,18] In this work, we attempted to incorporate carbamate-based hydrogen bonding motif into SP-containing monomer to render preorganization of SP moieties within polymersome bilayers and therefore enhance UV-actuated MC-MC cooperative interactions. Thus, SPA monomer was newly designed and facilely synthesized via the reaction of hydroxyl-functionalized SP with 2-isocyantoethyl methacrylate (Scheme S1a). As a control without hydrogen bonding interactions, an analogous SPO monomer containing a carbonate instead of carbamate linkage was also synthesized (Scheme S1b). The chemical structures of both SPA and SPO monomers were characterized by ^{1}H and ^{13}C NMR analysis and ESI-MS (Figures S1−S2). Next, reversible addition−fragmentation chain transfer (RAFT) polymerizations of SPA, SPO, and SPMA monomers were conducted using PEG_{45}-based macroRAFT agent, affording a series of photochromic amphiphilic BCPs with varying hydrophobic block lengths, PEO_{45}-*b*-$PSPA_x$ (x = 6, 19, and 27), PEO_{45}-*b*-$PSPO_y$ (y = 20), and PEO_{45}-*b*-$PSPMA_z$ (z = 7). These BCPs were characterized by ^{1}H NMR and GPC analysis (Figures S3−S4) and their structural parameters are summarized in Table 1.

Table 1. Structural Parameters of Photochromic Diblock Copolymers and Corresponding Morphologies of Self-Assembled Nanostructures in Aqueous Media

diblock copolymers	M_n[a] kDa	M_n[b] kDa	M_w/M_n[b]	aggregates morphology[c]	$\langle D_h\rangle$[d]/ nm	μ_2/Γ^{2}[d]
PEO_{45}-*b*-$PSPA_6$	5.2	4.7	1.21	Micelles	40	0.08
PEO_{45}-*b*-$PSPA_{19}$	11.6	10.2	1.18	Vesicles	450	0.06
PEO_{45}-*b*-$PSPA_{27}$	15.7	13.1	1.32	Vesicles	70	0.07
PEO_{45}-*b*-$PSPO_{20}$	12.4	11.3	1.24	Vesicles	430	0.06
PEO_{45}-*b*-$PSPMA_7$	5.1	4.7	1.13	Micelles	25	0.05

[a]Determined by ^{1}H NMR analysis. [b]Obtained from GPC analysis using DMF as eluent. [c]Determined by TEM, SEM, and AFM analysis. [d]Determined by dynamic laser light scattering analysis.

For as-synthesized PEO_{45}-*b*-$PSPA_x$, PEO_{45}-*b*-$PSPO_y$, and PEO_{45}-*b*-$PSPMA_z$, SP moieties are initially in the hydrophobic ring-closed state, and the amphiphilic nature renders them to spontaneously self-assemble in aqueous media. The self-assembly of PEO_{45}-*b*-$PSPA_x$ (x = 6, 19, and 27) was conducted by slowly adding water into the THF solution of BCPs at 25 °C. Specifically, PEO_{45}-*b*-$PSPA_6$ with the shortest PSPA block self-assembled into spherical nanoparticles with a hydro-

DOI: 10.1021/jacs.5b10127
J. Am. Chem. Soc. 2015, 137, 15262−15275

dynamic diameter, $\langle D_h \rangle$, of ~40 nm, whereas vesicular nanostructures were observed for PEO_{45}-*b*-$PSPA_{19}$ and PEO_{45}-*b*-$PSPA_{27}$ BCPs with longer PSPA blocks (Table 1 and Figure 1). The formed BCP vesicles should possess hydrophobic SP-containing bilayer membranes stabilized with both inner and outer PEO coronas.

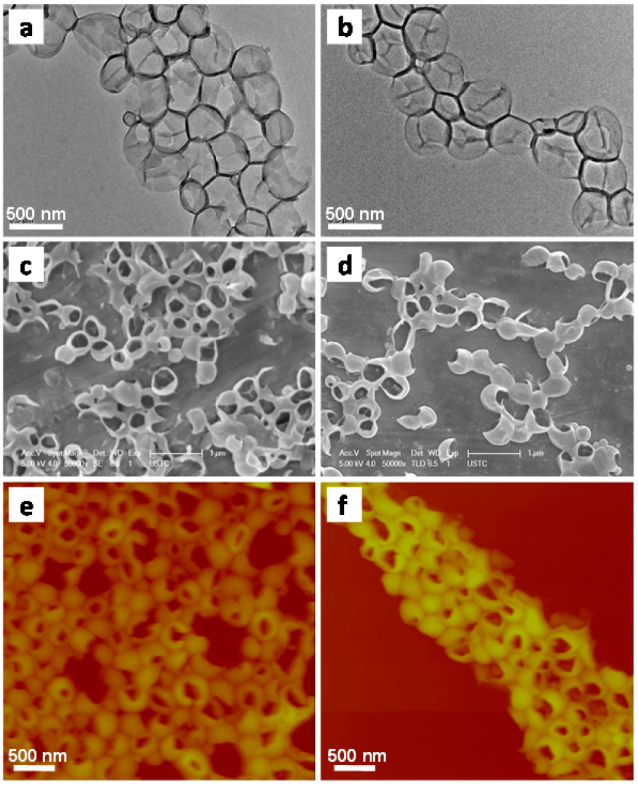

Figure 1. Microscopic characterization of PEO_{45}-*b*-$PSPA_{19}$ polymersomes before and after UV irradiation. (a,b) TEM images, (c,d) SEM images, and (e,f) AFM height images recorded for (a,c,e) as-prepared SP polymersomes (original and without UV irradiation) and (b,d,f) MC polymersomes (after being subjected to UV 365 nm irradiation for 10 min).

Typical transmission electron microscopy (TEM) images of PEO_{45}-*b*-$PSPA_{19}$ and PEO_{45}-*b*-$PSPA_{27}$ polymersomes are shown in Figure 1a and Figure S5, respectively, revealing that size dimension of the former was much larger than the latter. Furthermore, vesicular microstructure of PEO_{45}-*b*-$PSPA_{19}$ self-assemblies was also verified by scanning electron microscopy (SEM) and atomic force microscopy (AFM) (Figure 1c,e and Figure S6). Dynamic laser light scattering (LLS) analysis revealed that the polymersome dispersion of PEO_{45}-*b*-$PSPA_{19}$ exhibited an intensity-average hydrodynamic diameter, $\langle D_h \rangle$, of ~450 nm and a polydispersity (μ_2/Γ^2) of 0.06, whereas the $\langle D_h \rangle$ of PEO_{45}-*b*-$PSPA_{27}$ polymersomes was ~70 nm with a polydispersity of 0.07 (Table 1), which is in general agreement with TEM observations (Figures 1a and S5). The above results revealed that morphologies and size dimensions of self-assembled nanostructures can be tuned by adjusting hydrophobic block lengths.

Photoswitchable and Reversible Isomerization of Spiropyran Moieties in Photochromic Polymersomes. It is well-documented that SP derivatives are photoresponsive and transform into zwitterionic ring-opened MC derivatives under UV light irradiation. In addition, the SP-to-MC isomerization process is reversible and the reverse process can be actuated under visible light irradiation or extended annealing under dark conditions. The photochromic feature of SP moieties was then evaluated by UV−vis spectroscopy. For PEO_{45}-*b*-$PSPA_{19}$ unimers dissolved in THF, SP moieties were initially in the ring-closed form, exhibiting negligible absorbance in the range of 450−700 nm. However, prominently increased absorbance was observed after 1 min irradiation under a hand-held UV lamp (λ_1 = 365 nm; Figure S7a). The emerging absorption peak was centered at ~574 nm, corresponding to UV-triggered formation of zwitterionic MC residues. After incubating the UV-irradiated solution under dark conditions, the newly formed MC absorption peak gradually diminished and almost no absorbance can be detected after ~10 min incubation. This can be ascribed to spontaneous recovery of original ring-closed SP state (Figure S7a). These preliminary results suggested that the RAFT polymerization process and resultant diblock copolymers did not affect the photochromic feature of SP moieties. We further examined UV light-triggered SP-to-MC isomerization of PEO_{45}-*b*-$PSPA_{19}$ polymersomes self-assembled in aqueous milieu. As compared to the unimer state in THF (Figure S7a), much longer UV irradiation duration (~10 min) was needed for the SP-to-MC transition to reach final equilibrium state in the case of PEO_{45}-*b*-$PSPA_{19}$ polymersomes (Figure S8a); for example, 365 nm UV light irradiation for 2 min only leads to ~65% SP-to-MC transition (Figure 2a and Figure S8a−c).

Next, visible light-actuated MC-to-SP reverse transition was investigated. As expected, green light illumination (λ_2 = 530 nm) of UV-irradiated MC polymersome dispersion led to gradually attenuated MC absorption peak and the absorbance intensity stabilized out after >20 min λ_2 irradiation, and the half-life time ($t_{1/2}$) was ~3 min (Figure 2b,c and Figure S8d). Thus, visible light-actuated MC-to-SP transition for the polymersome dispersion was much slower than PEO_{45}-*b*-$PSPA_{19}$ in THF solution (~2 min λ_2 irradiation to complete; Figure S7b). We proposed that dense packing and partial alignment of SP moieties within polymersome bilayers, as well as synergistic MC-MC interactions (zwitterionic interactions and $\pi-\pi$ stacking interactions between coplanar MC residues with extended π-conjugation) should be responsible for the slower MC-to-SP reverse transition. We can also tell from Figure 2b that even after 20 min λ_2 irradiation, the MC absorption peak could not completely disappear, with ~12 mol % SP moieties still retaining in the ring-opened MC state (Figure 2c). On the other hand, UV-actuated SP-to-MC and visible light-actuated MC-to-SP processes for the polymersome dispersion could be repeated for several times without significant fatigue effect under alternated λ_1/λ_2 irradiation, as reflected by reversible changes in MC absorption intensities (Figure 2d).

Since the ring-opened zwitterionic MC form is generally less thermodynamically stable than the ring-closed SP form, the reverse MC-to-SP transition can also occur under dark conditions in a thermally driven manner. A striking feature was that MC moieties within UV-irradiated PEO_{45}-*b*-$PSPA_{19}$ polymersome bilayers exhibited extremely slow spontaneous MC-to-SP transition under dark conditions, with $t_{1/2}$ values being 26.1 and 22.4 h at 25 and 37 °C, respectively (Figure 2c and Figure S9a,b). For the control BCP with carbonate instead of carbamate side linkages, PEO_{45}-*b*-$PSPO_{20}$ polymersomes possessed $t_{1/2}$ of ~3.2 h at 25 °C and ~1 h at 37 °C under dark conditions (Figure S9c,d and Figure S10a), which was much

DOI: 10.1021/jacs.5b10127
J. Am. Chem. Soc. 2015, 137, 15262−15275

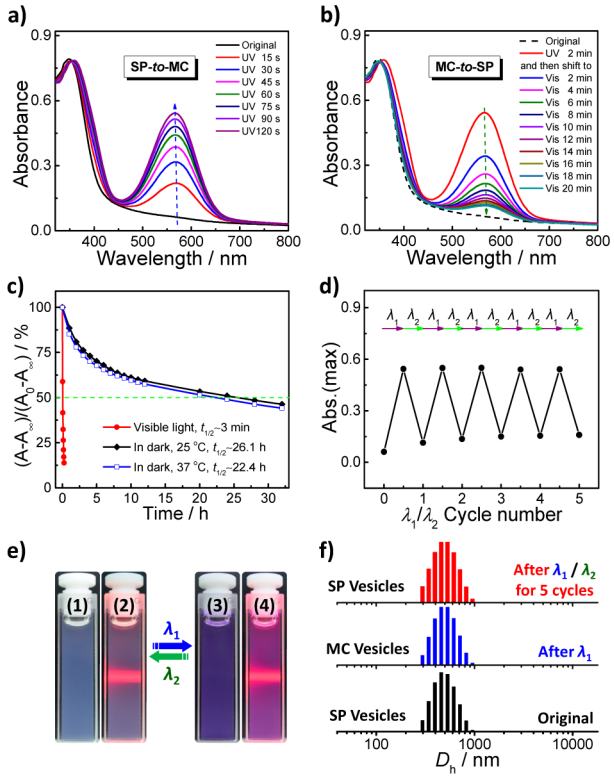

Figure 2. Reversible SP-MC isomerization of spiropyran moieties within polymersome bilayers. Irradiation time dependent absorbance spectra recorded for PEO_{45}-*b*-$PSPA_{19}$ polymersome dispersion upon (a) UV (λ_1, 365 nm; 1.5 mW/cm^2) and (b) green light (λ_2, 530 nm; 1 mW/cm^2) irradiation. (c) Kinetics of reverse isomerization of MC polymersomes (after 2 min UV irradiation) under λ_2 irradiation at 25 °C or dark conditions at 25 and 37 °C, respectively. A_0: initial MC absorbance at 565 nm after 2 min λ_1 irradiation; A_∞: absorbance of SP polymersome dispersion at 565 nm. (d) Absorption intensity changes (λ_{max} = 565 nm) during alternate λ_1/λ_2 irradiation cycles. (e) Macroscopic photographs of (1,3) vesicular dispersions and (2,4) the Tyndall effect under red light laser: (1,2) SP polymersomes (λ_2) and (3,4) MC polymersomes (λ_1). (f) Intensity-average hydrodynamic diameter, D_h, distributions recorded for dispersions of as-prepared SP polymersomes, MC polymersomes after λ_1 irradiation, and SP polymersomes after 5 repetitive λ_1/λ_2 irradiation cycles.

faster than those of PEO_{45}-*b*-$PSPA_{19}$ polymersomes. Thus, although both PEO_{45}-*b*-$PSPA_{19}$ and PEO_{45}-*b*-$PSPO_{20}$ BCPs could self-assemble into polymersomes with comparable $\langle D_h \rangle$ values (450 and 430 nm, respectively; Table 1), the packing of photochromic hydrophobic blocks and degree of orientation for corresponding MC moieties should be different within two types of polymersomes. Since the main difference between chemical structures of PEO_{45}-*b*-$PSPA_{19}$ and PEO_{45}-*b*-$PSPO_{20}$ was the presence of carbamate linkages in the former while carbonate linkages in the latter (Scheme S1), we reasoned that carbamate-incurred hydrogen bonding interactions within PEO_{45}-*b*-$PSPA_{19}$ polymersomes should be mainly responsible.

To determine whether MC moieties within polymersome bilayers exhibited H-type or J-type stacking, at first we measured absorption spectra of UV-irradiated THF solutions of PEO_{45}-*b*-$PSPA_{19}$ and PEO_{45}-*b*-$PSPO_{20}$ BCPs. It was quite unexpected that the former possessed an absorption maximum at ~574 nm, whereas the latter exhibited an absorption maximum at ~589 nm (Figure S10c). Since corresponding SPA and SPO monomers possessed quite similar absorption properties in THF solution (Figure S10d),[22] we speculate that at the molecularly dissolved single chain level, hydrogen bonding interactions between neighboring carbamate linkages could promote more ordered stacking between MC moieties, leading to the blue shift of MC absorption.[22] To the best of our knowledge, directly obtaining evidence of hydrogen bonding-assisted intrachain packing of chromophores has been unprecedented, and this feature deserves to be further explored.

On the other hand, UV-irradiated MC polymersome dispersions of PEO_{45}-*b*-$PSPA_{19}$ and PEO_{45}-*b*-$PSPO_{20}$ exhibited absorption maxima at ~567 nm and ~578 nm, respectively (Figure S10b). Thus, MC moieties within UV-irradiated PEO_{45}-*b*-$PSPA_{19}$ and PEO_{45}-*b*-$PSPO_{20}$ polymersomes both exhibited H-type stacking to some extent, relative to those in their molecularly dissolved state (~574 nm and ~589 nm, respectively; Figure S10c).[21,22] Moreover, a direct comparison between MC absorption properties of UV-irradiated PEO_{45}-*b*-$PSPA_{19}$ and PEO_{45}-*b*-$PSPO_{20}$ polymersomes led us to conclude that carbamate side linkage-involved hydrogen bonding interactions in the former could facilitate more regular packing of MC moieties, i.e., further blue shift in the absorption maximum, presumably due to prealignment of ring-closed SP moieties within polymersome bilayers. Note that the ordered packing of MC moieties could further strengthen cooperative noncovalent interactions (hydrogen bonding, zwitterionic, and $\pi-\pi$ stacking interactions) in a positive feedback manner, which should help stabilize MC polymersomes upon UV irradiation (Scheme 1).

To further clarify the effects of side chain hydrogen bonding interactions and morphology of self-assembled aggregates on the kinetics of spontaneous MC-to-SP transition and MC stacking modes, we investigated micelles ($\langle D_h \rangle$ ~ 40 nm) self-assembled from PEO_{45}-*b*-$PSPA_6$ BCP with shorter PSPA block (Table 1). The results (Figures S11–S12, see Supporting Information for detailed discussions, page S23) clearly indicated H-stacking modes of MC moieties within self-assembled micelles upon UV irradiation.[21,22] For PEO_{45}-*b*-$PSPA_{19}$ vesicles and PEO_{45}-*b*-$PSPA_6$ micelles, UV-actuated MC moieties exhibited absorption maxima of 567 and 557 nm, respectively. Initially, we had envisaged that PEO_{45}-*b*-$PSPA_{19}$ polymersome bilayers should exhibit more apparent blue shift, as compared to the radial chain packing module within PEO_{45}-*b*-$PSPA_6$ micelles. As shown in Figure S8a,b and Figure S13, upon 2 min UV irradiation, the extent of SP-to-MC transition for aqueous dispersions of PEO_{45}-*b*-SPA_{19} polymersomes and PEO_{45}-*b*-SPA_6 micelles were determined to be ~65% and ~64%, respectively. Considering the similar microenvironments of SPA moieties, the above results implied that in PEO_{45}-*b*-$PSPA_6$ micelles, MC residues exhibited higher degree of chromophore orientation and packing. This might be ascribed to the shorter PSPA block length for PEO_{45}-*b*-$PSPA_6$ and elevated chain flexibility within micellar cores due to lower glass transition temperature. On the other hand, for PEO_{45}-*b*-$PSPMA_7$ BCP in which the conventional ester functionality-containing SPMA monomer lacks hydrogen bonding motif (Scheme S1), the unimer solution in THF and micelles in aqueous media exhibited MC maxima of ~586 nm and ~569 nm upon UV irradiation (~17 nm blue shift in the micellar state; Figure S12; see Supporting Information for detailed discussions, page S23).

We also compared MC absorption maxima and MC-to-SP transition kinetics for PEO_{45}-*b*-$PSPA_{19}$ polymersomes and micellar nanoparticles fabricated via cosolvent self-assembly

DOI: 10.1021/jacs.5b10127
J. Am. Chem. Soc. 2015, 137, 15262–15275

and nanoprecipitation techniques, respectively (Figure S8 and S14). Intriguingly, upon UV irradiation, micellar nanoparticles exhibited prominent red-shift of the MC absorption (574 nm), as compared to that of polymersomes (559 nm). Moreover, $t_{1/2}$ values of reverse MC-to-SP transition under dark conditions for micellar nanoparticles were considerably lower than those of polymersomes (8.7 h vs 26.1 h at 25 °C and 3.0 h vs 22.4 h at 37 °C). These results clearly indicated the crucial role of SP preorganization within self-assembled polymersomes. We tentatively ascribed this feature to further enhanced H-stacking of MC species by existing synergistic MC-MC interactions. This seems reasonable considering that every repeating unit within the PSPMA block contains one photochromic chromophore moiety.

Apart from different photochromic features and SP-to-MC transition kinetics between PEO_{45}-*b*-$PSPA_{19}$ solution in THF and polymersome dispersion in aqueous media, their fluorescence emission behaviors were also different. In the molecularly dissolved state, PEO_{45}-*b*-$PSPA_{19}$ copolymer in THF possessed negligible fluorescence emission initially, however, after UV irradiation, significantly enhanced fluorescence emission ascribing to ring-opened MC moieties was observed and reversibly switchable fluorescence emission could be achieved under alternate UV−vis light irradiation (Figure S15). In contrast, vesicular aggregates in aqueous media only exhibited negligible emission turn-on upon UV irradiation (Figure S15), although light-actuated SP-to-MC transition did occur. The weak fluorescence emission of MC polymersomes was likely due to the very high local concentration of MC moieties within bilayer membranes. In addition, the H-type stacking between MC residues resulting from synergistic zwitterionic and $\pi-\pi$ interaction led to more prominent emission quenching.

Structural Integrity of Photochromic Polymersomes upon UV−Vis Light Irradiation. The previous section discussed reversible spectroscopic (e.g., UV−vis absorbance and fluorescence) properties of photochromic polymersomes under alternate λ_1/λ_2 light irradiation. UV light-triggered formation of zwitterionic MC moieties for the PEO_{45}-*b*-$PSPA_{19}$ polymersome dispersion was accompanied by a distinct color change from bluish tinge characteristic of colloidal dispersion to navy blue, which can be readily discerned by the naked eye (Figure 2e). Moreover, for the polymersome dispersion before and after UV irradiation, clearly evident Tyndall effects could be both observed (Figure 2e), suggesting that PEO_{45}-*b*-$PSPA_{19}$ polymersomes remained as colloidal aggregates upon UV-triggered SP-to-MC transition. Furthermore, ^{1}H NMR spectra of the polymersome dispersion before and after UV irradiation also verified the aggregated state since only signals of well-solvated PEO coronas were evident (Figure S16). Moreover, TEM, SEM, and AFM observations of PEO_{45}-*b*-$PSPA_{19}$ polymersomes after UV irradiation revealed the presence of almost intact vesicular nanostructures (Figure 1b,d,f). Dynamic LLS measurements indicated that the $\langle D_h \rangle$ of polymersomes remained almost unchanged after UV irradiation (Figure 2f). All the above results demonstrated that PEO_{45}-*b*-$PSPA_{19}$ polymersomes possessed unprecedented microstructural stability after UV and visible light irradiation although light-regulated reversible SP-to-MC transition did occur (Figure 2a,b). Note that in previous reports concerning micellar nanostructures self-assembled from SPMA-containing block or random copolymers, UV-triggered SP-to-MC transition typically led to micellar disintegration or microstructural rearrangement.[13c,16a,c,18]

In order to further elucidate this issue, time-dependent dynamic LLS measurements were conducted to follow the evolution of scattering light intensity and $\langle D_h \rangle$ during UV irradiation (Figure S17a). The scattering intensity of PEO_{45}-*b*-$PSPA_{19}$ polymersome dispersion exhibited an initial ∼20% increase within ∼40 s UV irradiation and then leveled off at later stages, whereas no apparent changes in $\langle D_h \rangle$ could be discerned in the entire irradiation period (2 min). UV irradiation at extended duration (10 min) rendered no appreciable changes (Figure S18), although almost all SP moieties should have been transformed into MC residues (Figure S8a). UV-triggered formation of zwitterionic MC moieties within vesicle bilayers and microenvironmental polarity switching should lead to partial swelling and size increase, thus, the constant $\langle D_h \rangle$ during UV irradiation was quite unexpected. The initial abrupt increase (within 40 s UV irradiation) in scattering intensity was also perplexing. We speculated that SP polymersome and MC polymersome dispersions might possess different refractive index increment (dn/dc) values. This was indeed proved to be true, and dn/dc values were determined to be 0.147 mL/g for as-prepared SP polymersomes and 0.174 mL/g for UV-irradiated MC polymersomes (Figure S19). Therefore, the initial increase in scattered light intensity under λ_1 irradiation can be ascribed to increased dn/dc value for the MC polymersome dispersion.

On the other hand, weight-average molar masses (M_w) of SP polymersomes and UV-irradiated MC polymersomes were determined to be 2.87×10^9 g/mol and 3.00×10^9 g/mol, respectively, by static LLS measurements (Figure S20). Considering that zwitterionic MC moieties are hydrophilic and the contribution of tightly bound water molecules, we tentatively concluded that the aggregation number (N_{agg}) per polymersome remained constant upon UV triggered SP-to-MC transition. This was also in agreement with dynamic LLS results (Figure 2f). These results revealed that no fusion/fission between polymersomes or chain exchange between polymersomes and unimer chains occurred upon UV irradiation. On the basis of the M_w value of SP polymersomes, N_{agg} was calculated to be $\sim 2.1 \times 10^5$. If we took an average diameter of ∼400 nm and bilayer wall thickness of ∼13 nm for SP polymersomes, as determined by cryo-TEM (Figure 3a), the local concentration of SP moieties within bilayer membrane was estimated to be ∼1.08 mol/L. If we assumed homogeneous distribution of SP moieties within bilayers, the average distance between neighboring SP residues was ∼1.15 nm. Such a local high concentration is highly advantageous for enhancing synergistic MC-MC interactions.

As shown above, UV light-induced SP-to-MC isomerization within PEO_{45}-*b*-$PSPA_{19}$ polymersomes did not compromise the structural integrity of polymersomes. Then the reverse process, visible light-actuated MC-to-SP transition should result in recovery of original polymersomes with SP in the ring-closed state (Figure 2b). Upon alternate UV and visible light irradiation of the polymersome dispersion, both MC absorption intensities (Figure 2c) and scattering light intensities (Figure S17c) exhibited periodic increase and decrease. A closer check of time-dependent changes in scattering intensities during visible light irradiation revealed that the reverse process was more gradual and took ∼10 min to level off, as compared to ∼40 s needed for the UV-triggered reverse process (Figure S17a,b). Again, $\langle D_h \rangle$ of polymersomes did not exhibit any

DOI: 10.1021/jacs.5b10127
J. Am. Chem. Soc. 2015, 137, 15262−15275

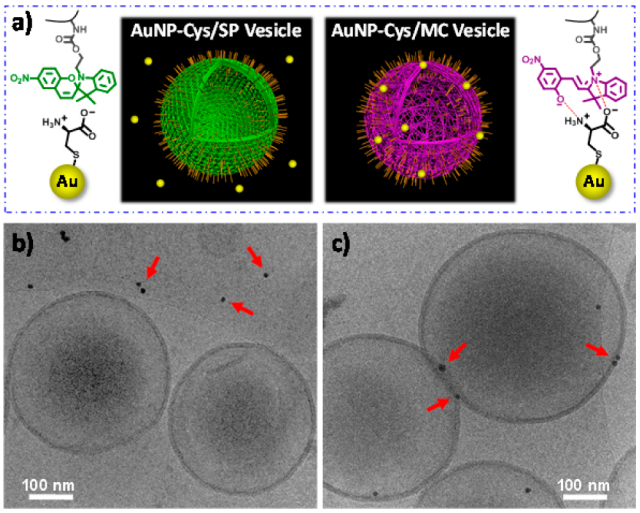

Figure 3. (a) Schematic illustration of light-triggered reversible anchoring of cysteine-functionalized Au NPs at the surface of polymersomes upon alternate λ_1/λ_2 light irradiation. (b,c) Cryo-TEM images recorded for PEO_{45}-*b*-$PSPA_{19}$ polymersome dispersion (0.05 g/L) in the presence of cysteine-functionalized Au NPs (12 nm; 0.01 g/L) after being subjected to (b) green light (λ_2, SP polymersomes) and (c) UV light (λ_1, MC polymersomes) irradiation, respectively. Light: λ_1 = 365 nm, 1.5 mW/cm^2; λ_2 = 530 nm, 1 mW/cm^2; 25 °C.

appreciable changes during the reverse process (Figure S18b), and the vesicular nanostructure remained unchanged after five repetitive UV and visible light irradiation cycles, as confirmed by TEM observation (Figure S17d).

The above results led us to conclude that PEO_{45}-*b*-$PSPA_{19}$ polymersomes exhibited reversible photochromic transition upon UV and visible light irradiation and retained in the vesicular microstructure. We then attempted to further verify the generation of zwitterionic MC moieties within bilayer membranes and confirm that zwitterionic interactions (i.e., paired ionic interactions) were also responsible for MC-MC interactions, in addition to well-established $\pi-\pi$ stacking interactions between MC species. Previous reports indicated that zwitterionic ring-opened MC residues favorably interact with amino acids (e.g., phenylalanine and cysteine) and MC encapsulated within liposome bilayers could facilitate transmembrane transport of zwitterionic small molecule substances.[20] For PEO_{45}-*b*-$PSPA_{19}$ polymersomes, the hydrophobic bilayer was shielded by PEO coronas. For the mixture of PEO_{45}-*b*-$PSPA_{19}$ polymersomes and phenylalanine (Phe) in deuterium oxide (D_2O), SP moieties in polymersomes were supposed to exhibit no specific interactions with Phe prior to UV irradiation. Thus, ^{1}H NMR signals of *Ar*-H originating from free Phe was employed as an internal standard (Figure S21). After in situ UV light-induced SP-to-MC transition, remarkably decreased *Ar*-H signals were discerned. This implied that free Phe molecules were adsorbed onto polymersome bilayers due to paired electrostatic interactions between zwitterionic Phe and ring-opened MC moieties.

The above ^{1}H NMR results can serve as an indirect evidence for the generation of MC bilayers upon UV irradiation. To directly visualize specific paired electrostatic interactions and the integrity of vesicular nanostructures after UV irradiation, additional cryo-TEM experiments were conducted to probe the system in the vitrified and frozen-hydrated state. Cysteine-functionalized 12 nm Au NPs costabilized by PEO and cysteine were prepared via ligand exchange procedures (Figure S22). For the mixture of PEO_{45}-*b*-$PSPA_{19}$ polymersome dispersion and cysteine-stabilized Au NPs, although Au NPs possessed an intensive absorbance peak at ~520 nm, it did not adversely affect the SP-to-MC isomerization process under UV irradiation (Figure S23). Cyro-TEM observations revealed that no Au NPs were apparently bound to the polymersome surface before UV irradiation. In sharp contrast, after 2 min UV light exposure, Au NPs were found to be selectively attached at the surface of bilayer membranes (Figure 3). Again, we cannot discern any disruption of polymersome microstructures after UV irradiation. These results clearly confirmed that UV-generated MC moieties exhibit paired electrostatic interactions with zwitterionic guest molecules, which can be utilized for further functional explorations.

Stabilization of Photoswitchable Polymersomes by Cooperative Noncovalent Interactions. The above results established that PEO_{45}-*b*-$PSPA_{19}$ polymersomes could retain structural integrity upon UV-triggered SP-*to*-MC transition (Scheme 1), which is in stark contrast to previous report concerning conventional SPMA-containing amphiphilic copolymers.[13c,16a,c,18] For as-prepared polymersomes, since SP moieties are in the hydrophobic ring-closed state, their microstructural stability was maintained by hydrophobic and carbamate-involved hydrogen bonding interactions; note that $\pi-\pi$ interactions between SP residues are relatively weak due to the noncoplanar nature. For UV-actuated MC polymersomes, vesicular microstructures were maintained by weakened hydrophobic interactions, hydrogen bonding interactions, and synergistically enhanced $\pi-\pi$ and zwitterionic interactions. As confirmed by spectroscopic evidence, carbamate-involved hydrogen bonding interactions leads to preorganization of SP moieties within bilayer membranes, facilitating H-stacking of MC residues (Figure S8–S13). Within polymersomes, hydrogen bonding, $\pi-\pi$ stacking, and paired ionic interactions can cooperatively self-enhance and synergistically contribute to the MC polymersomes stability.

To further understand the cooperativity of multiple noncovalent interactions and screen for essential elements in maintaining polymersome microstructures, we conducted a series of control experiments. Both $\pi-\pi$ stacking and zwitterionic interactions were involved between MC-MC moieties, although previous literature reports mainly ascribe MC-MC interactions to the $\pi-\pi$ stacking type.[21] Since $\pi-\pi$ interactions should be inert to pH variation and zwitterionic interactions rely on the extent of ionization of phenolic hydroxyl in MC, we examined the polymersome stability at varying pH conditions. pH titration experiments revealed that MC phenolic hydroxyl moieties possessed an apparent pK_a of ~1.5 (Figure S24), which was lower than the previously reported pK_a value (~2.2) for small molecule MC in a two-phase system.[23] Dynamic LLS analysis revealed that scattered light intensities experienced negligible changes in range of pH 3.0–7.0, whereas an abrupt decrease in the scattered intensity was observed at pH < 3.0 (Figure 4a), which was in line with the apparent pK_a of MC species in polymersomes. The dramatic decrease in scattered light intensity in acidic milieu (i.e., pH < 3.0) was presumably due to pH-induced disassembly of MC polymersomes. The formation of cationic MCH$^+$ upon protonation was also clearly evident with an apparent colorimetric transition from navy blue at pH 7.0–3.0 to yellowish at pH 1.0 (inset in Figure 4a).

DOI: 10.1021/jacs.5b10127
J. Am. Chem. Soc. 2015, 137, 15262–15275

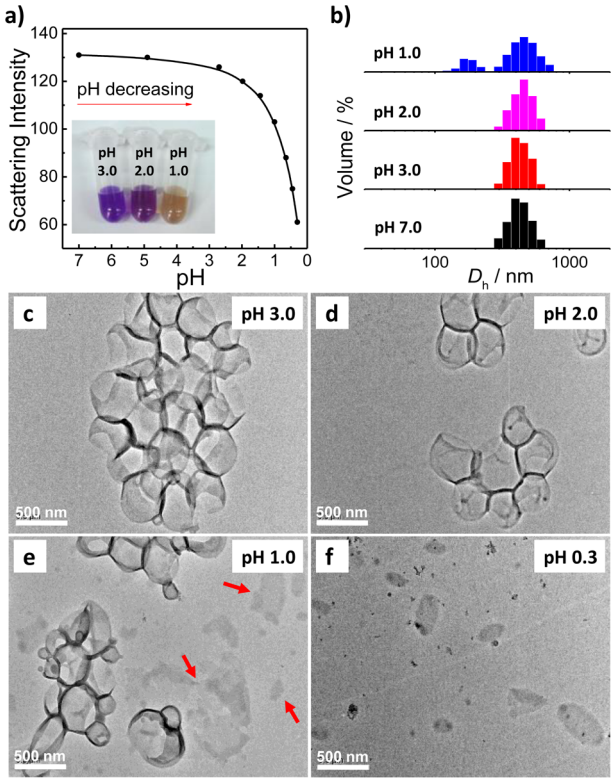

Figure 4. pH-dependent (a) scattered light intensity and (b) volume-average hydrodynamic diameter distributions, D_h, recorded for PEO_{45}-*b*-$PSPA_{19}$ polymersome dispersions after being subjected to 10 min UV irradiation (SP polymersomes). The inset in (a) shows macroscopic photographs of MC polymersome dispersions in aqueous media at varying pH (pH 3.0, 2.0, and 1.0, respectively). (c,d,e,f) TEM images of MC polymersomes in aqueous media at (c) pH 3.0, (d) pH 2.0, (e) pH 1.0, and (f) pH 0.3, respectively.

Meanwhile, the $\langle D_h \rangle$ of MC polymersomes exhibited negligible changes in the pH range of 2.0−7.0, and disintegrated aggregates were observed at pH 1.0 with >50% extent of protonation for MC moieties (Figure 4b). When the pH was further decreased to ∼0.3, no polymersomes could exist anymore (Figure S25). These dynamic LLS results also agreed well with TEM observations. The vesicular morphology was retained at both pH 3.0 and pH 2.0, whereas irregular aggregates coexisting with vesicles started to appear at pH 1.0 and no polymersomes could be discerned at pH 0.3 (Figure 4c−4f). These results confirmed that UV-triggered zwitterionic MC state was of crucial importance in maintaining the integrity of vesicular nanostructures. $\pi-\pi$ stacking interactions between protonated MC residues should partially persist, although charge repulsion between MCH^+ residues might weaken them to some extent. Thus, both $\pi-\pi$ stacking and paired ionic interactions between zwitterionic MC moieties could synergistically contribute to polymersome stability. Note that within bilayer membranes, the local MC concentration was roughly estimated to be ∼1.08 mol/L, which were advantageous toward effective MC-MC interactions facilitated and preorganized by side chain carbamate hydrogen bonding interactions. We can also tell from Figure 4 that photochromic polymersomes either in the SP or MC state could endure physiological pH gradients (typically in the range of pH 4.5−8.0).[24]

In order to clarify the contribution of carbamate-incurred hydrogen bonding interactions toward the stabilization of MC polymersomes, we compared the microstructural stability of PEO_{45}-*b*-$PSPA_{19}$ polymersomes with PEO_{45}-*b*-$PSPO_{20}$ polymersomes during UV irradiation. Note that in the latter case, side chain hydrogen bonding interactions did not exist, although partial H-type MC-MC stacking could occur within UV-irradiated PEO_{45}-*b*-$PSPO_{20}$ polymersomes (Figures S9−S10). In contrast to the excellent stability of PEO_{45}-*b*-$PSPA_{19}$ polymersomes, it was found that PEO_{45}-*b*-$PSPO_{20}$ polymersomes collapsed into irregular aggregates after 10 min UV light irradiation (Figure 5). We further probed this process by AFM

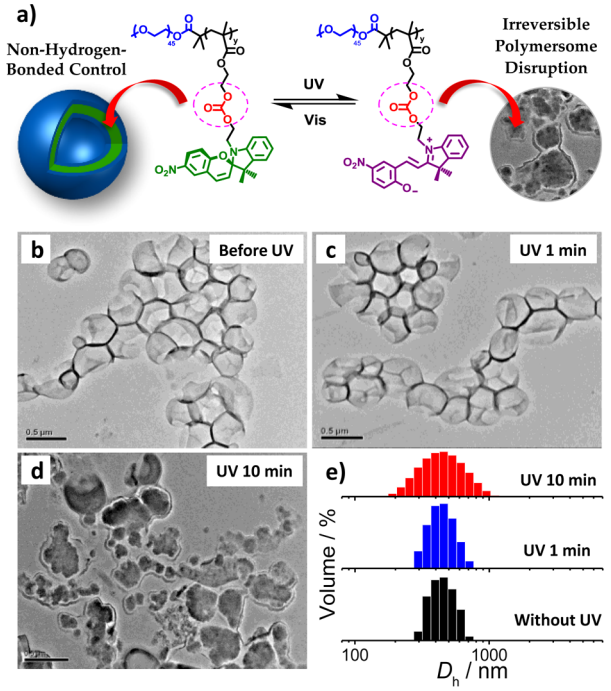

Figure 5. (a) UV−visible (λ_1/λ_2) light irradiation triggers reversible photochromic SP-MC transition within PEO_{45}-*b*-$PSPO_{20}$ polymersomes, leading to irreversible morphological transformation into irregular aggregates. PEO_{45}-*b*-$PSPO_{20}$ serves as a reference control for polymersomes without carbamate hydrogen bonding motifs within hydrophobic bilayers, as opposed to polymersomes of PEO_{45}-*b*-$PSPA_{19}$. (b,c,d) TEM images of PEO_{45}-*b*-$PSPO_{20}$ polymersomes (b) without, and with (c) 1 min and (d) 10 min UV 365 nm irradiation, respectively. (e) UV irradiation time-dependent evolution of volume-average hydrodynamic diameter distributions, D_h, recorded for PEO_{45}-*b*-$PSPO_{20}$ polymersomes.

analysis (Figure S26). For PEO_{45}-*b*-$PSPA_{19}$ polymersomes containing hydrogen bonding motif, not only the polymersomes nanostructure could be well maintained upon UV-actuated SP-to-MC transition, but also the average height profile of polymersomes significantly increased form ∼150 nm to ∼255 nm, suggesting that UV irradiation actually led to more robust polymersomes with zwitterionic bilayers. On the other hand, for PEO_{45}-*b*-$PSPO_{20}$ polymersomes lacking of hydrogen bonding interactions, the polymersomes with an initial AFM height profile of ∼90 nm exhibited complete collapse into irregular aggregates (Figure S26d).

To further verify that carbamate-incurred hydrogen bonding interactions were indeed present, we utilized in situ temperature dependent FT-IR spectroscopy to probe PEO_{45}-*b*-$PSPA_{19}$ polymersomes directly fabricated in D_2O. As shown in Figure S27, for the polymersome dispersion before and after UV irradiation at 25 °C, carbamate N−H stretching exhibited a

DOI: 10.1021/jacs.5b10127
J. Am. Chem. Soc. 2015, 137, 15262−15275

broad band at ~3412 and ~3410 cm^{-1}, respectively, which then gradually shifted to higher wavenumbers (~3449 and ~3428 cm^{-1}) upon elevating the temperature to 70 °C. These results confirmed that carbamate-incurred hydrogen bonding interactions are indeed present within both SP and MC polymersomes. On the other hand, UV irradiation duration-dependent evolution of scattered light intensity for PEO_{45}-*b*-$PSPO_{20}$ polymersomes was also drastically different (Figure S28), as compared to that of PEO_{45}-*b*-$PSPA_{19}$ polymersomes (Figure S18). These results clearly revealed that hydrogen bonding interactions along with $\pi-\pi$ stacking and zwitterionic interactions were all of vital importance in stabilizing PEO_{45}-*b*-$PSPA_{19}$ polymersomes in the UV-triggered MC state.

The mechanism of cooperative noncovalent interactions in reinforcing photoswitchable polymersomes was further explored by quantifying the structural stability with critical aggregation concentration (CAC) values.[7b] In general, CAC values primarily depend on hydrophobic block lengths for amphiphilic block copolymers with the same hydrophilic block. Quite unexpectedly, we found that hydrogen bonding interactions could also exhibit significant effects. More specifically, the CAC value of PEO_{45}-*b*-$PSPA_{19}$ polymersomes was determined to be 5.3×10^{-5} g/L by dynamic LLS, which was roughly 1 order of magnitude lower than that of PEO_{45}-*b*-$PSPO_{20}$ polymersomes (3.2×10^{-4} g/L) without hydrogen bonding motifs (Figure S29). Interestingly, after UV light irradiation, the CAC value of PEO_{45}-*b*-$PSPA_{19}$ polymersomes was decreased by half to ~2.5×10^{-5} g/L, suggesting that cooperative noncovalent interactions actually reinforced the vesicular nanostructure. On the other hand, the CAC value of PEO_{45}-*b*-$PSPO_{20}$ polymersomes increased more than twice to ~7.0×10^{-4} g/L after UV irradiation (Figure S29), which was in agreement with UV-triggered polymersome disassembly (Figure 5).

Aiming to provide further insights concerning the effect of hydrogen bonding interactions on the bilayer membrane stability, Langmuir films of PEO_{45}-*b*-$PSPA_{19}$ and PEO_{45}-*b*-$PSPO_{20}$ BCPs at the air−water interface were fabricated to mimic vesicular bilayers and surface pressure changes as a function of molecular area were monitored (Figure S30). After UV irradiation, the molecular area of PEO_{45}-*b*-$PSPA_{19}$ film increased from 860 $Å^2$ to 1170 $Å^2$, revealing that the monolayer structure was retained without being dissolved into the water subphase; in addition, UV irradiation actually led to the formation of more robust monolayer film (Figure S30a). This was also consistent with decreased CAC value (Figure S29a). On the other hand, we could not discern any appreciable changes in molecular areas for PEO_{45}-*b*-$PSPO_{20}$ monolayers prepared under identical conditions before and after UV irradiation (Figure S30b).

The above-discussed cooperative noncovalent interactions involving hydrogen bonding and synergistic zwitterionic/$\pi-\pi$ stacking interactions should also work for PEO_{45}-*b*-$PSPA_6$ micelles, in addition to PEO_{45}-*b*-$PSPA_{19}$ vesicles. For comparison, conventional SPMA-based amphiphilic block copolymer without hydrogen bonding motifs, PEO_{45}-*b*-$PSPMA_7$, was also utilized (Scheme S1c). Both PEO_{45}-*b*-$PSPA_6$ and PEO_{45}-*b*-$PSPMA_7$ BCPs self-assembled into spherical micelles, as confirmed by TEM results (Figure S31a and S32a; Table 1). Upon UV irradiation, the scattered light intensity of PEO_{45}-*b*-$PSPA_6$ micellar dispersion increased abruptly at the beginning and then quickly stabilized out (Figure S33a), and micellar sizes remained almost the same (Figure S33b). Thus, cooperative noncovalent interactions within UV-actuated PEO_{45}-*b*-$PSPA_6$ micelles in the MC state were also of robust structural stability (Figures S31−S32). These results were quite comparable to the retaining of vesicular nanostructure of PEO_{45}-*b*-$PSPA_{19}$ polymersomes under UV irradiation. In sharp contrast, PEO_{45}-*b*-$PSPMA_7$ micelles consisting of conventional single ester-based SPMA monomer without carbamate linkage failed to maintain the original micellar morphology and started to disassemble upon UV irradiation (Figures S32b−d and Figure S34), presumably due to the absence of SP preorganization facilitated by cooperative hydrogen bonding interactions. CAC measurements further revealed that hydrogen bonding interactions could prominently decrease CAC values for micellar assemblies. Specifically, before and after UV irradiation, the CACs of PEO_{45}-*b*-$PSPA_6$ micelles were ~150 times and ~200 times lower than those of PEO_{45}-*b*-$PSPMA_7$ micelles, respectively (Figure S35).

Reversibly Photoswitching Polymersome Permeability and Spatiotemporally Controlled Intracellular Payload Release. The previous sections established that UV−vis light irradiation can actuate reversible transformation between hydrophobic SP and hydrophilic zwitterionic MC moieties within polymersome bilayers. Cooperative noncovalent interactions in both SP and MC polymersomes endow them with microstructural stability. For MC polymersomes, the stability was partially enhanced due to synergistic $\pi-\pi$ stacking and zwitterionic interactions, as well as hydrogen bonding and weakened hydrophobic interactions. We envisaged that reversible SP-to-MC transition could lead to reversible permeability changes of bilayer membranes. To verify this assumption, first, coumarin 102, a microenvironmental polarity-sensitive dye was loaded into initially hydrophobic bilayers of SP polymersomes. Prior to UV light irradiation, an intensive fluorescence emission was observed due to that the fluorescent probe was encapsulated within hydrophobic bilayers (Figure 6a). Without UV irradiation, no time-dependent changes in emission intensity could be discerned (Figure 6b). Nevertheless, considerable decrease in fluorescence intensity was clearly evident with the onset of UV irradiation. This was presumably due to UV-triggered generation of hydrophilic zwitterionic MC residues, leading to hydrophobicity-to-hydrophilicity transition of polymersome bilayers. This feature could be further utilized for triggered corelease of hydrophobic and hydrophilic substance, like small molecule drugs.[11]

Aside from hydrophobic payloads, the aqueous interior of polymersomes could also be facilely loaded with hydrophilic anticancer drugs and controlled release of payloads could be actuated by UV light-induced SP-to-MC isomerization. Since the hydrophilicity of UV-irradiated polymersomes was endowed by zwitterionic MC moieties, which were conjugated onto polymeric backbones via carbamate linkages, and the average distance between neighboring MC species was calculated to be ~1.15 nm (Figure S20), we could envisage that the zwitterionic MC bilayer membrane should be highly selective toward the molar mass, polarity, and types of charges of small molecule payloads. At first, a hydrophilic anticancer drug, 2′-deoxy-5-fluorouridine (5-dFu), was chosen as a small molecule model drug and light-mediated release of 5-dFu was investigated (Figure 6c and 6d). After encapsulating into the aqueous lumen of polymersomes during self-assembly, the release profile of 5-dFu from original SP polymersomes and MC polymersomes were continuously monitored by UV−vis

DOI: 10.1021/jacs.5b10127
J. Am. Chem. Soc. 2015, 137, 15262−15275

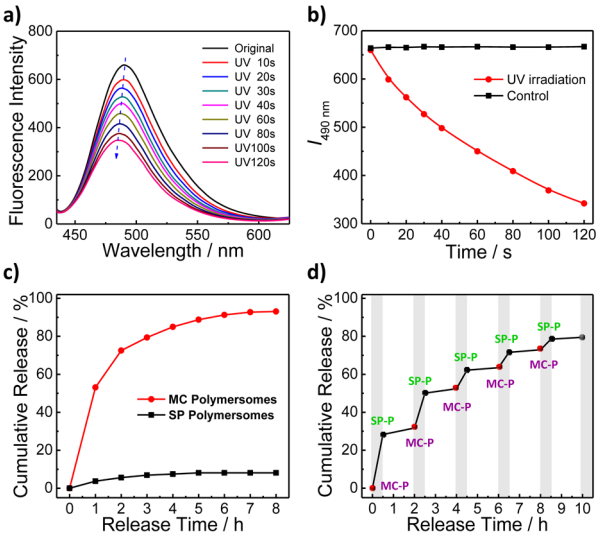

Figure 6. Light-triggered switching of polymersome permeability. (a) Fluorescence spectra and (b) emission intensity changes (490 nm) recorded for the aqueous dispersion of PEO_{45}-*b*-$PSPA_{19}$ polymersomes upon UV-actuated SP-MC transition, and coumarin-102 as a polarity-sensitive probe was encapsulated within polymersome bilayers. (c) Release profiles of hydrophilic anticancer drug (2′-deoxy-5-fluorouridine, 5-dFu) from as-prepared SP polymersomes and MC polymersomes actuated by 2 min UV irradiation. (d) Ladder-type controlled release profiles of 5-dFu from polymersomes upon alternate UV light (λ_1, 2 min) and green light (λ_2, 15 min) irradiation; gray regions highlight rapid release stages after λ_1 irradiation, and blank regions show slow release stages after λ_2 irradiation.

spectroscopy. Specifically, over 90% of 5-dFu was released from UV-irradiated MC polymersomes within 8 h, as compared to <10% 5-dFu release from SP polymersomes during the same time period (Figure 6c). Note that the release experiments were actuated by 2 min UV irradiation to render the formation of MC polymersomes. The unexpected slow MC-to-SP transition for MC polymersomes under dark conditions ($t_{1/2} \sim 22.4$ h at 37 °C, Figure S10a) is quite advantageous for future in vivo drug delivery applications, given that the drug release process could be actuated via short UV irradiation duration. It can be also deduced that the drug release rate will decrease at later stages due to elevated extent of MC-to-SP transition. This new type of self-regulated and self-constrained release mechanism could be further exploited to design next generation delivery nanocarriers.

Moreover, the release of 5-dFu could be programmed and readily switched by alternate UV (λ_1 = 365 nm) and visible light (λ_2 = 530 nm) irradiation (Figure 6d). 5-dFu can be efficiently released from UV-actuated MC polymersomes due to SP-to-MC transition, whereas the release was almost prohibited upon visible light irradiation. Thus, photoswitchable drug release could be repeated for many times and a ladder-type controlled release profile was obtained under alternate λ_1/λ_2 irradiation (Figure 6d). These results clearly confirmed light-regulated and switchable bilayer permeability. However, in spite of elevated permeability upon SP-to-MC transition, not all hydrophilic molecules could be released from the aqueous lumen of polymersomes after UV irradiation. For instance, neither doxorubicin hydrochloride (DOX·HCl, 580 Da; positively charged) nor calcein dye (623 Da, negatively charged) could be released from MC polymersomes (Figure S36), presumably due to their larger molecular size compared to 5-dFu (246 Da).

Encouraged by in vitro photoswitchable permeability of polymersome bilayers and tunable release of selective payloads, we then attempted to achieve reversible polymersome bilayer permeability switching within living cells and programmed intracellular payload release. Hydrophilic small molecule DAPI (4′,6-diamidino-2-phenylindole, 277 Da; positively charged), a cell nuclei DNA-intercalating dye with blue emission, was chosen to be encapsulated into the aqueous interior of polymersomes; upon intracellular release from polymersomes, DAPI will spontaneously enter into cell nuclei and report the extent of release through enhanced fluorescence emission. To verify that DPAI release was solely due to light-regulated bilayer permeability switching in living HeLa cells instead of polymersome disintegration, a bilayer membrane-impermeable macromolecular dye, Texas red-labeled dextran (dextran-TR, 10 kDa), was simultaneously encapsulated into the aqueous lumen of polymersomes (Figure S37).

After endocytosis of DAPI/dextran-TR coencapsulated polymersomes, the intracellular photoswitching process was investigated by confocal laser scanning microscopy (CLSM). As shown in Figure 7, one cell in the white square box was arbitrarily chosen to be irradiated by alternate λ_1/λ_2 irradiation (designating 405 and 543 nm laser scanning as λ_1 and λ_2, respectively), and other cells in the frame were left unirradiated, serving as a control. Interestingly, within the irradiation square area, emerging blue fluorescence emission of DNA-bound DAPI within the cell nucleus was observed under alternate λ_1/λ_2 laser irradiation. On the contrary, without 405 nm irradiation, no apparent blue emission in the cell nuclei of control cells could be discerned. Further quantitative analysis revealed that under alternate 405/543 nm laser scanning, the DAPI emission intensity gradually increased in a ladder-type manner (Figure 7). These results suggested that original or visible light-actuated SP polymersomes exhibited low membrane permeability and effectively restrained DAPI release. Prominently increased permeability of polymersome bilayers and efficient DAPI release could be achieved through 405 nm laser scanning-triggered SP-to-MC transition.

Finally, in order to explore the generality and validity of permeability switching while maintaining the microstructural stability by taking advantage of cooperative noncovalent interactions and reversible SP-to-MC transition, we fabricated microcapsule reactors of PEO_{45}-*b*-$PSPA_{27}$ BCP with the size comparable to cells. This enabled direct observation of permeability tuning under CLSM conditions. We postulated that if the photochromic feature could be inherited in the microcapsule system with quite thick membrane layer, light-regulated switching of membrane permeability should allow for selective diffusion of specific substances, mimicking the cellular transport process. By virtue of a previously reported coaxial electrospray microfluidics technique,[25] microcapsules with a uniform size of ~75 μm were fabricated. It was found that successive 405 nm laser light scanning of microcapsules could actuate SP-*to*-MC isomerization without disintegration of microcapsule structures (Figure S38).

In order to probe whether light-induced SP-to-MC isomerization could lead to elevated permeability for the microcapsule membrane, two categories of quinone-cyanine based NIR fluorescence probes, BQCy-1 and BQCy-2, were designed and synthesized (Scheme S2 and Figure S39). Initially non-fluorescent BQCy-1 and BQCy-2 could respond to thiol

DOI: 10.1021/jacs.5b10127
J. Am. Chem. Soc. 2015, 137, 15262−15275

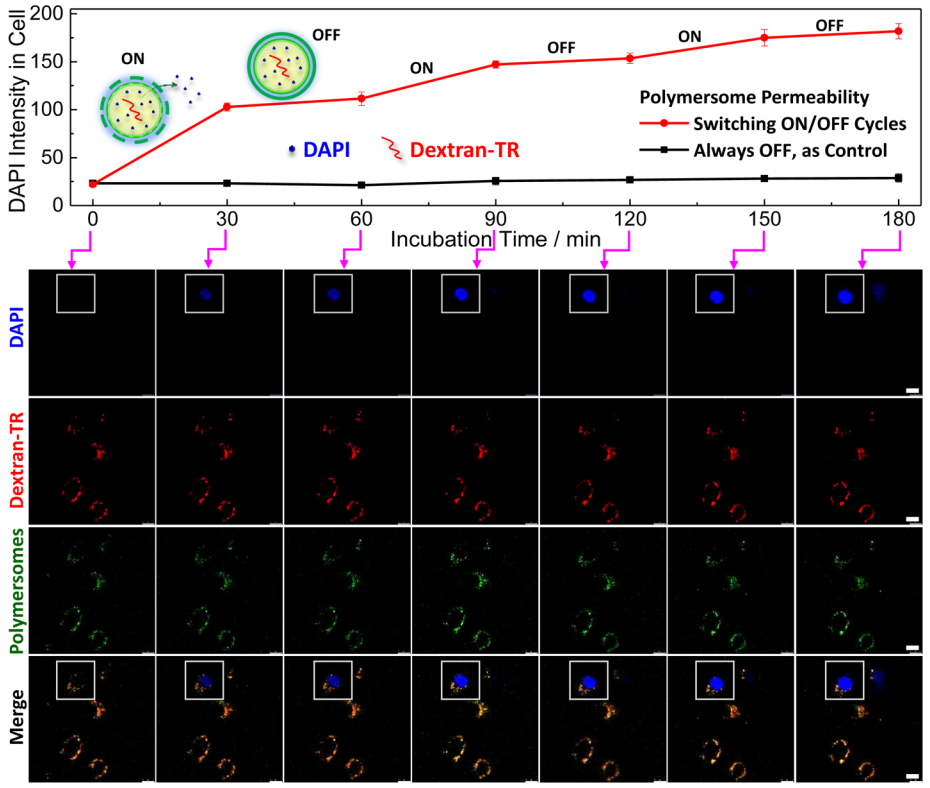

Figure 7. Polymersome permeability switching in living cells. (Bottom) Representative CLSM images of blue (DAPI, 450−470 nm), red (600−630 nm; dextran-TR: Texas Red-labeled dextran; 10 kDa, encapsulated within polymersomes), and green (630−700 nm, PEO_{45}-*b*-$PSPA_{19}$ polymersomes) channels, and merged images recorded for HeLa cells after irradiating the white square box region with λ_1 = 405 nm laser light for 2 scans at time points of 0, 60, and 120 min and λ_2 = 543 nm laser light for 10 scans at time points of 30, 90, and 150 min, respectively. (Top) Alternate 405 and 543 nm laser light irradiation-actuated polymersome permeability switching and programmed intracellular cumulative DAPI release (red line) inside the irradiated square box area; as a control, the evolution of DAPI intensity outside the square box region was also plotted (black line). In all experiments, HeLa cells were incubated for 4 h in the presence of PEO_{45}-*b*-$PSPA_{19}$ polymersomes coencapsulating dextran-TR and DAPI; after washing and replacing with fresh DMEM medium, the culture mixture was further incubated for 8 h. Scale bar is 10 μm.

compounds and pH with prominent emission turn-on features, respectively (Figure S40).[26] Specifically, the emission turn-on of BQCy-1 in the presence of thiol-containing molecules (e.g., cysteine and glutathione) was confirmed by fluorescence spectroscopy (Figure S41). In contrast, the introduction of cystine without free thiol moieties led to negligible increase in emission intensity (Figure S41b). On the other hand, the fluorescence emission of BQCy-2 dye was highly dependent on pH and can selectively report solution pH (Figures S42−S43).

To mimic the cellular transport of amino acids by taking advantage of light-mediated microcapsule permeability changes, we constructed microcapsule reactors by encapsulating thiol-responsive BQCy-1 probe inside the internal aqueous cavity. Upon addition of 1 mM cysteine (as a model zwitterionic amino acid) into the microcapsule dispersion, the evolution of fluorescence emission was monitored by CLSM. As shown in Figure S44, without 405 nm laser irradiation, fluorescence emissions of BQCy-1 both inside and outside microcapsules were very weak during the 60 min incubation period, suggesting that microcapsule membrane in the SP state were impermeable to both cysteine (121 Da) and BQCy-1 probe (1006 Da), i.e., both of them cannot diffuse across the hydrophobic membrane bilayers.

However, after being irradiated with 405 nm laser light, SP-to-MC isomerization within microcapsule membranes led to efficient emission turn-on of encapsulated BQCy-1 due to the diffusion of cysteine across the microcapsule membrane (Figure 8a). The fluorescence emission of BQCy-1 inside microcapsules gradually increased by extending the incubation duration (0−60 min; Figure 8b). This indicated that initially impermeable microcapsules were transformed to be selectively permeable toward small molecules such as cysteine. Note that the transport of zwitterionic cysteine could be further facilitated by zwitterionic interactions with ring-opened MC moieties.[20] A closer check of Figure 8b told us that the emission turn-on of BQCy-1 was the most prominent at the membrane, as compared to the inner interior of microcapsule reactors. This feature was reasonable considering that both nonfluorescent BQCy-1 and highly fluorescent thiol-reacted product possess zwitterionic charged nature, which should assist their effective adsorption onto the UV-actuated MC membrane. Note that due to the relatively large molar mass of zwitterionic BQCy-1 (1006 Da), it was retained inside the microcapsule. Similarly, light-regulated diffusion of hydrated protons through photochromic microcapsules could also be achieved by utilizing microcapsule reactors encapsulating pH-responsive BQCy-2 fluorescent probes (Figure S45). Again, fluorescence intensities at the membranes was much higher than the microcapsule interior due to zwitterionic (paired ionic) interactions of BQCy-2 with ring-opened MC residues at the surface of inner membrane leaflets.

DOI: 10.1021/jacs.5b10127
J. Am. Chem. Soc. 2015, 137, 15262−15275

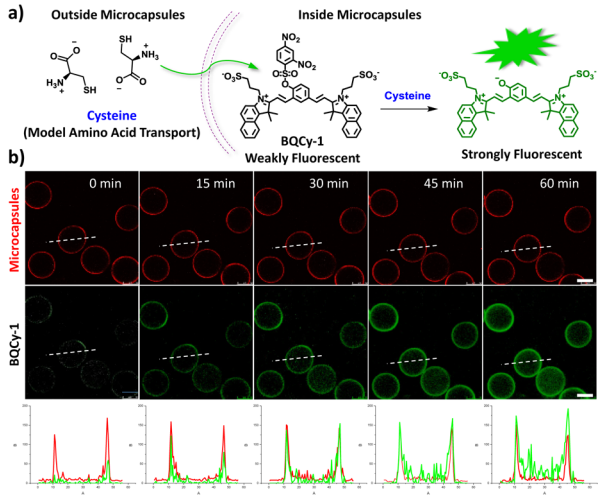

Figure 8. Light-triggered switching of microcapsule permeability toward the transport of zwitterionic amino acid species. (a) Schematic illustration of cysteine transport (as a model amino acid) from outside through the membrane of UV-irradiated PEO_{45}-*b*-$PSPA_{27}$ microcapsules and then turn on the fluorescence emission of encapsulated BQCy-1 (cysteine-reactive fluorogenic dye). (b) CLSM images recorded at varying incubation duration (0−60 min) for BQCy-1 encapsulated microcapsules of PEO_{45}-*b*-$PSPA_{27}$, which were coincubated with cysteine (1 mM) at first and then irradiated with 405 nm laser light for 2 scans. The red channel emission was collected at 630−700 nm for ring-opened spiropyran (MC) under 590 nm laser light excitation, and the green channel emission was collected at 700−750 nm for BQCy-1 under 633 nm laser light excitation. Scale bar is 50 μm.

CONCLUSIONS

Photochromic polymersomes exhibiting photoswitchable and reversible bilayer permeability were fabricated from amphiphilic PEO-*b*-PSPA block copolymers, where SPA is spiropyran (SP)-based monomer containing a unique carbamate linkage. SP moieties within self-assembled polymersome bilayers undergo phototriggered reversible isomerization between hydrophobic spiropyran (SP, λ_2 > 450 nm irradiation) and zwitterionic merocyanine (MC, λ_1 < 420 nm irradiation) states. Carbamate-incurred hydrogen bonding interactions led to preorganization of SP moieties within polymersome bilayers and elevated extent of H-type stacking of UV-triggered MC species, as compared to control block copolymers of SP monomer with a carbonate linkage. As opposed to the structural instability of self-assembled aggregates of conventional SP-containing amphiphilic copolymers upon UV irradiation, MC polymersomes of PEO-*b*-PSPA were stabilized by multiple cooperative noncovalent interactions including hydrophobic, hydrogen bonding, $\pi-\pi$ stacking, and paired electrostatic (zwitterionic) interactions, which mutually enhance each other in a positive feedback manner. Additional control experiments verified that carbamate-relevant hydrogen bonding interactions in PEO-*b*-PSPA are vital for microstructural stabilization of polymersomes in the zwitterionic MC state.

Moreover, reversible phototriggered SP-to-MC polymersome transition leads to membrane polarity and permeability switching from being nonimpermeable to selectively permeable toward small molecule species below critical molar masses. Hydrogen bonding motifs and other synergistic noncovalent interactions within PEO-*b*-PSPA polymersome bilayers results in unexpectedly slow MC-to-SP transition kinetics with $t_{1/2}$ > 20 h under dark conditions; thus, sustained payload release can be actuated after short duration UV irradiation. On the other hand, programmed and spatiotemporal intracellular drug release from structurally intact polymersomes was facilely achieved under alternate UV−vis light irradiation. By utilizing the design criteria of cooperative noncovalent interactions, PEO-*b*-PSPA microcapsule reactors were also constructed, possessing comparable photoregulated membrane permeability features. To the best of our knowledge, this work represents the first report of polymersomes exhibiting both reversible bilayer permeability switching and enhanced microstructural stability endowed by cooperative noncovalent interactions. In addition, the excellent permselectivity of bilayer membranes and switchable release modules (sustained versus on-demand release) of photochromic polymersomes augurs well for their future in vivo drug delivery applications.

ASSOCIATED CONTENT

Supporting Information

The Supporting Information is available free of charge on the ACS Publications website at DOI: 10.1021/jacs.5b10127.

Full experimental details, NMR, ESI-MS, UV−vis, fluorescence spectra, GPC, dynamic and static LLS, additional TEM, SEM, and CLSM images, and control experiments. (PDF)

AUTHOR INFORMATION

Corresponding Author

*sliu@ustc.edu.cn

Notes

The authors declare no competing financial interest.

ACKNOWLEDGMENTS

The financial support from National Natural Scientific Foundation of China (NNSFC) Project (21274137 and 51033005), Fundamental Research Funds for the Central Universities, and Specialized Research Fund for the Doctoral Program of Higher Education (SRFDP, 20123402130010).

REFERENCES

(1) (a) Engelman, D. M. *Nature* **2005**, *438*, 578−580. (b) Murata, K.; Mitsuoka, K.; Hirai, T.; Walz, T.; Agre, P.; Heymann, J. B.; Engel, A.; Fujiyoshi, Y. *Nature* **2000**, *407*, 599−605.

(2) (a) Hill, J. P.; Jin, W. S.; Kosaka, A.; Fukushima, T.; Ichihara, H.; Shimomura, T.; Ito, K.; Hashizume, T.; Ishii, N.; Aida, T. *Science* **2004**, *304*, 1481−1483. (b) Hartgerink, J. D.; Beniash, E.; Stupp, S. I. *Science* **2001**, *294*, 1684−1688. (c) Graff, A.; Sauer, M.; Van Gelder, P.; Meier, W. *Proc. Natl. Acad. Sci. U. S. A.* **2002**, *99*, 5064−5068. (d) Zhu, J. H.; Zhang, S. Y.; Zhang, K.; Wang, X. J.; Mays, J. W.; Wooley, K. L.; Pochan, D. J. *Nat. Commun.* **2013**, *4*, 2297. (e) Yan, D. Y.; Zhou, Y. F.; Hou, J. *Science* **2004**, *303*, 65−67. (f) Mabrouk, E.; Cuvelier, D.; Brochard-Wyart, F.; Nassoy, P.; Li, M. H. *Proc. Natl. Acad. Sci. U. S. A.* **2009**, *106*, 7294−7298. (g) Yan, Q.; Zhao, Y. *Angew. Chem., Int. Ed.* **2013**, *52*, 9948−9951. (h) Kim, H.; Jeong, S. M.; Park, J. W. *J. Am. Chem. Soc.* **2011**, *133*, 5206−5209. (i) Wang, C.; Chen, Q. S.; Xu, H. P.; Wang, Z. Q.; Zhang, X. *Adv. Mater.* **2010**, *22*, 2553−2555. (j) Liu, G. J.; Wyman, I. *Nat. Chem.* **2013**, *5*, 733−734. (k) Lee, I. H.; Shin, S.; Choi, T. L. *Science* **2015**, *347*, 1310−1311. (l) Yu, S. Y.; Azzam, T.; Rouiller, I.; Eisenberg, A. *J. Am. Chem. Soc.* **2009**, *131*, 10557−10566. (m) Hu, J. M.; Zhang, G. Q.; Liu, S. Y. *Chem. Soc. Rev.* **2012**, *41*, 5933−5949. (n) Rao, J. Y.; Khan, A. *J. Am. Chem. Soc.* **2013**, *135*, 14056−14059. (o) Alswieleh, A. M.; Cheng, N.; Canton, I.; Ustbas, B.; Xue, X.; Ladmiral, V.; Xia, X.; Ducker, R. E.; Zubir, O. E.; Cartron, M. L.; Hunter, C. N.; Leggett, G. J.; Armes, S. P. *J. Am. Chem. Soc.* **2014**,

DOI: 10.1021/jacs.5b10127
J. Am. Chem. Soc. 2015, 137, 15262−15275

136, 9404−9413. (p) Grayson, S. M.; Frechet, J. M. J. *Chem. Rev.* **2001**, *101*, 3819−3867. (q) Liu, M. J.; Kono, K.; Frechet, J. M. J. *J. Controlled Release* **2000**, *65*, 121−131. (r) Hawker, C. J.; Lee, R.; Frechet, J. M. J. *J. Am. Chem. Soc.* **1991**, *113*, 4583−4588. (s) Lux, C. D.; Joshi-Barr, S.; Nguyen, T.; Mahmoud, E.; Schopf, E.; Fomina, N.; Almutairi, A. *J. Am. Chem. Soc.* **2012**, *134*, 15758−15764. (t) Hu, J. M.; Liu, S. Y. *Acc. Chem. Res.* **2014**, *47*, 2084−2095. (u) Li, Y. M.; Yu, H. S.; Qian, Y. F.; Hu, J. M.; Liu, S. Y. *Adv. Mater.* **2014**, *26*, 6734−6741. (v) Hu, X. L.; Liu, G. H.; Li, Y.; Wang, X. R.; Liu, S. Y. *J. Am. Chem. Soc.* **2015**, *137*, 362−368. (w) Hu, J. M.; Zhang, G. Y.; Ge, Z. S.; Liu, S. Y. *Prog. Polym. Sci.* **2014**, *39*, 1096−1143.

(3) (a) Sun, G.; Fang, H. F.; Cheng, C.; Lu, P.; Zhang, K.; Walker, A. V.; Taylor, J. S. A.; Wooley, K. L. *ACS Nano* **2009**, *3*, 673−681. (b) Li, Y.; Lokitz, B. S.; McCormick, C. L. *Angew. Chem., Int. Ed.* **2006**, *45*, 5792−5795. (c) Chandrawati, R.; Caruso, F. *Langmuir* **2012**, *28*, 13798−13807. (d) Liu, G. H.; Wang, X. R.; Hu, J. M.; Zhang, G. Y.; Liu, S. Y. *J. Am. Chem. Soc.* **2014**, *136*, 7492−7497. (e) Checot, F.; Lecommandoux, S.; Gnanou, Y.; Klok, H. A. *Angew. Chem., Int. Ed.* **2002**, *41*, 1339−1343. (f) Howse, J. R.; Jones, R. A. L.; Battaglia, G.; Ducker, R. E.; Leggett, G. J.; Ryan, A. J. *Nat. Mater.* **2009**, *8*, 507−511. (g) Battaglia, G.; Ryan, A. J. *J. Am. Chem. Soc.* **2005**, *127*, 8757−8764. (h) Yan, Q.; Yuan, J. Y.; Cai, Z. N.; Xin, Y.; Kang, Y.; Yin, Y. W. *J. Am. Chem. Soc.* **2010**, *132*, 9268−9270. (i) Yan, B.; Tong, X.; Ayotte, P.; Zhao, Y. *Soft Matter* **2011**, *7*, 10001−10009. (j) Vriezema, D. M.; Hoogboom, J.; Velonia, K.; Takazawa, K.; Christianen, P. C. M.; Maan, J. C.; Rowan, A. E.; Nolte, R. J. M. *Angew. Chem., Int. Ed.* **2003**, *42*, 772−776. (k) Antonietti, M.; Forster, S. *Adv. Mater.* **2003**, *15*, 1323−1333. (l) Kim, K. T.; Zhu, J. H.; Meeuwissen, S. A.; Cornelissen, J. J. L. M.; Pochan, D. J.; Nolte, R. J. M.; van Hest, J. C. M. *J. Am. Chem. Soc.* **2010**, *132*, 12522−12524. (m) Hu, J. M.; Wu, T.; Zhang, G. Y.; Liu, S. Y. *J. Am. Chem. Soc.* **2012**, *134*, 7624−7627.

(4) (a) Discher, D. E.; Ortiz, V.; Srinivas, G.; Klein, M. L.; Kim, Y.; David, C. A.; Cai, S. S.; Photos, P.; Ahmed, F. *Prog. Polym. Sci.* **2007**, *32*, 838−857. (b) Wang, K.; Guo, D. S.; Wang, X.; Liu, Y. *ACS Nano* **2011**, *5*, 2880−2894. (c) Yu, G. C.; Zhou, X. R.; Zhang, Z. B.; Han, C. Y.; Mao, Z. W.; Gao, C. Y.; Huang, F. H. *J. Am. Chem. Soc.* **2012**, *134*, 19489−19497. (d) Meng, F. H.; Zhong, Z. Y.; Feijen, J. *Biomacromolecules* **2009**, *10*, 197−209. (e) Lomas, H.; Canton, I.; MacNeil, S.; Du, J.; Armes, S. P.; Ryan, A. J.; Lewis, A. L.; Battaglia, G. *Adv. Mater.* **2007**, *19*, 4238−4243. (f) Duan, Q. P.; Cao, Y.; Li, Y.; Hu, X. Y.; Xiao, T. X.; Lin, C.; Pan, Y.; Wang, L. Y. *J. Am. Chem. Soc.* **2013**, *135*, 10542−10549. (g) Hu, X. L.; Hu, J. M.; Tian, J.; Ge, Z. S.; Zhang, G. Y.; Luo, K. F.; Liu, S. Y. *J. Am. Chem. Soc.* **2013**, *135*, 17617−17629.

(5) (a) Wilson, D. A.; Nolte, R. J. M.; van Hest, J. C. M. *Nat. Chem.* **2012**, *4*, 268−274. (b) Vriezema, D. M.; Garcia, P. M. L.; Oltra, N. S.; Hatzakis, N. S.; Kuiper, S. M.; Nolte, R. J. M.; Rowan, A. E.; van Hest, J. C. M. *Angew. Chem., Int. Ed.* **2007**, *46*, 7378−7382. (c) Chen, Q.; Schonherr, H.; Vancso, G. J. *Small* **2009**, *5*, 1436−1445.

(6) (a) Tanner, P.; Baumann, P.; Enea, R.; Onaca, O.; Palivan, C.; Meier, W. *Acc. Chem. Res.* **2011**, *44*, 1039−1049. (b) Marguet, M.; Bonduelle, C.; Lecommandoux, S. *Chem. Soc. Rev.* **2013**, *42*, 512−529. (c) Ben-Haim, N.; Broz, P.; Marsch, S.; Meier, W.; Hunziker, P. *Nano Lett.* **2008**, *8*, 1368−1373.

(7) (a) Discher, B. M.; Won, Y. Y.; Ege, D. S.; Lee, J. C. M.; Bates, F. S.; Discher, D. E.; Hammer, D. A. *Science* **1999**, *284*, 1143−1146. (b) Discher, D. E.; Eisenberg, A. *Science* **2002**, *297*, 967−973. (c) Sauer, M.; Haefele, T.; Graff, A.; Nardin, C.; Meier, W. *Chem. Commun.* **2001**, 2452−2453.

(8) (a) Kumar, M.; Habel, J. E. O.; Shen, Y. X.; Meier, W. P.; Walz, T. *J. Am. Chem. Soc.* **2012**, *134*, 18631−18637. (b) Yan, Q.; Wang, J. B.; Yin, Y. W.; Yuan, J. Y. *Angew. Chem., Int. Ed.* **2013**, *52*, 5070−5073. (c) Broz, P.; Driamov, S.; Ziegler, J.; Ben-Haim, N.; Marsch, S.; Meier, W.; Hunziker, P. *Nano Lett.* **2006**, *6*, 2349−2353. (d) Kim, K. T.; Cornelissen, J. J. L. M.; Nolte, R. J. M.; van Hest, J. C. M. *Adv. Mater.* **2009**, *21*, 2787−2791. (e) Amstad, E.; Kim, S. H.; Weitz, D. A. *Angew. Chem., Int. Ed.* **2012**, *51*, 12499−12503. (f) Jochum, F. D.; Theato, P. *Chem. Soc. Rev.* **2013**, *42*, 7468−7483. (g) Roy, D.; Cambre, J. N.; Sumerlin, B. S. *Prog. Polym. Sci.* **2010**, *35*, 278−301. (h) Gohy, J. F.; Zhao, Y. *Chem. Soc. Rev.* **2013**, *42*, 7117−7129. (i) Ge, Z. S.; Liu, S. Y. *Chem. Soc. Rev.* **2013**, *42*, 7289−7325. (j) Shum, H. C.; Kim, J. W.; Weitz, D. A. *J. Am. Chem. Soc.* **2008**, *130*, 9543−9549. (k) Dong, R. J.; Zhu, B. S.; Zhou, Y. F.; Yan, D. Y.; Zhu, X. Y. *Angew. Chem., Int. Ed.* **2012**, *51*, 11633−11637. (l) Gaitzsch, J.; Appelhans, D.; Wang, L. G.; Battaglia, G.; Voit, B. *Angew. Chem., Int. Ed.* **2012**, *51*, 4448−4451. (m) Bellomo, E. G.; Wyrsta, M. D.; Pakstis, L.; Pochan, D. J.; Deming, T. J. *Nat. Mater.* **2004**, *3*, 244−248. (n) Napoli, A.; Valentini, M.; Tirelli, N.; Muller, M.; Hubbell, J. A. *Nat. Mater.* **2004**, *3*, 183−189. (o) Chiu, H. C.; Lin, Y. W.; Huang, Y. F.; Chuang, C. K.; Chern, C. S. *Angew. Chem., Int. Ed.* **2008**, *47*, 1875−1878.

(9) Spulber, M.; Najer, A.; Winkelbach, K.; Glaied, O.; Waser, M.; Pieles, U.; Meier, W.; Bruns, N. *J. Am. Chem. Soc.* **2013**, *135*, 9204−9212.

(10) (a) Helmy, S.; Leibfarth, F. A.; Oh, S.; Poelma, J. E.; Hawker, C. J.; de Alaniz, J. R. *J. Am. Chem. Soc.* **2014**, *136*, 8169−8172. (b) Klajn, R.; Bishop, K. J. M.; Grzybowski, B. A. *Proc. Natl. Acad. Sci. U. S. A.* **2007**, *104*, 10305−10309. (c) Zhang, F.; Wang, L. P.; Brauner, M.; Liewald, J. F.; Kay, K.; Watzke, N.; Wood, P. G.; Bamberg, E.; Nagel, G.; Gottschalk, A.; Deisseroth, K. *Nature* **2007**, *446*, 633−639. (d) Tsai, Y. H.; Essig, S.; James, J. R.; Lang, K.; Chin, J. W. *Nat. Chem.* **2015**, *7*, 554−561. (e) Banghart, M.; Borges, K.; Isacoff, E.; Trauner, D.; Kramer, R. H. *Nat. Neurosci.* **2004**, *7*, 1381−1386. (f) Schroeder, A.; Goldberg, M. S.; Kastrup, C.; Wang, Y. X.; Jiang, S.; Joseph, B. J.; Levins, C. G.; Kannan, S. T.; Langer, R.; Anderson, D. G. *Nano Lett.* **2012**, *12*, 2685−2689. (g) Klajn, R.; Bishop, K. J. M.; Fialkowski, M.; Paszewski, M.; Campbell, C. J.; Gray, T. P.; Grzybowski, B. A. *Science* **2007**, *316*, 261−264. (h) Pieroni, O.; Fissi, A.; Angelini, N.; Lenci, F. *Acc. Chem. Res.* **2001**, *34*, 9−17.

(11) Wang, X. R.; Liu, G. H.; Hu, J. M.; Zhang, G. Y.; Liu, S. Y. *Angew. Chem., Int. Ed.* **2014**, *53*, 3138−3142.

(12) (a) Irie, M.; Fukaminato, T.; Sasaki, T.; Tamai, N.; Kawai, T. *Nature* **2002**, *420*, 759−760. (b) Kundu, P. K.; Samanta, D.; Leizrowice, R.; Margulis, B.; Zhao, H.; Borner, M.; Udayabhaskararao, T.; Manna, D.; Klajn, R. *Nat. Chem.* **2015**, *7*, 646−652. (c) Xie, X. J.; Crespo, G. A.; Mistlberger, G.; Bakker, E. *Nat. Chem.* **2014**, *6*, 202−207. (d) Xie, X. J.; Bakker, E. *J. Am. Chem. Soc.* **2014**, *136*, 7857−7860. (e) Friedle, S.; Thomas, S. W. *Angew. Chem., Int. Ed.* **2010**, *49*, 7968−7971. (f) Wagner, N.; Theato, P. *Polymer* **2014**, *55*, 3436−3453. (g) Zhang, Y.; Swaminathan, S.; Tang, S. C.; Garcia-Amoros, J.; Boulina, M.; Captain, B.; Baker, J. D.; Raymo, F. M. *J. Am. Chem. Soc.* **2015**, *137*, 4709−4719. (h) Davis, D. A.; Hamilton, A.; Yang, J. L.; Cremar, L. D.; Van Gough, D.; Potisek, S. L.; Ong, M. T.; Braun, P. V.; Martinez, T. J.; White, S. R.; Moore, J. S.; Sottos, N. R. *Nature* **2009**, *459*, 68−72. (i) Osborne, E. A.; Jarrett, B. R.; Tu, C. Q.; Louie, A. Y. *J. Am. Chem. Soc.* **2010**, *132*, 5934−5935. (j) Li, C. H.; Zhang, Y. X.; Hu, J. M.; Cheng, J. J.; Liu, S. Y. *Angew. Chem., Int. Ed.* **2010**, *49*, 5120−5124. (k) Ito, Y.; Sugimura, N.; Kwon, O. H.; Imanishi, Y. *Nat. Biotechnol.* **1999**, *17*, 73−75. (l) Shiraishi, Y.; Shirakawa, E.; Tanaka, K.; Sakamoto, H.; Ichikawa, S.; Hirai, T. *ACS Appl. Mater. Interfaces* **2014**, *6*, 7554−7562.

(13) (a) Tong, R.; Chiang, H. H.; Kohane, D. S. *Proc. Natl. Acad. Sci. U. S. A.* **2013**, *110*, 19048−19053. (b) Tong, R.; Hemmati, H. D.; Langer, R.; Kohane, D. S. *J. Am. Chem. Soc.* **2012**, *134*, 8848−8855. (c) Son, S.; Shin, E.; Kim, B. S. *Biomacromolecules* **2014**, *15*, 628−634.

(14) Sheng, L.; Li, M. J.; Zhu, S. Y.; Li, H.; Xi, G.; Li, Y. G.; Wang, Y.; Li, Q. S.; Liang, S. J.; Zhong, K.; Zhang, S. X. A. *Nat. Commun.* **2014**, *5*, 3044.

(15) (a) Hu, D. H.; Tian, Z. Y.; Wu, W. W.; Wan, W.; Li, A. D. Q. *J. Am. Chem. Soc.* **2008**, *130*, 15279−15281. (b) Yan, J.; Zhao, L. X.; Li, C.; Hu, Z.; Zhang, G. F.; Chen, Z. Q.; Chen, T.; Huang, Z. L.; Zhu, J. T.; Zhu, M. Q. *J. Am. Chem. Soc.* **2015**, *137*, 2436−2439. (c) Zhu, M. Q.; Zhang, G. F.; Li, C.; Aldred, M. P.; Chang, E.; Drezek, R. A.; Li, A. D. Q. *J. Am. Chem. Soc.* **2011**, *133*, 365−372.

(16) (a) Lee, H. I.; Wu, W.; Oh, J. K.; Mueller, L.; Sherwood, G.; Peteanu, L.; Kowalewski, T.; Matyjaszewski, K. *Angew. Chem., Int. Ed.* **2007**, *46*, 2453−2457. (b) Klajn, R. *Chem. Soc. Rev.* **2014**, *43*, 148−184. (c) Yan, B.; He, J.; Ayotte, P.; Zhao, Y. *Macromol. Rapid Commun.* **2011**, *32*, 972−976.

DOI: 10.1021/jacs.5b10127
J. Am. Chem. Soc. 2015, 137, 15262−15275

(17) Zhu, M. Q.; Zhu, L. Y.; Han, J. J.; Wu, W. W.; Hurst, J. K.; Li, A. D. Q. *J. Am. Chem. Soc.* **2006**, *128*, 4303−4309.
(18) (a) Yu, L. X.; Liu, Y.; Chen, S. C.; Guan, Y.; Wang, Y. Z. *Chin. Chem. Lett.* **2014**, *25*, 389−396. (b) Menon, S.; Ongungal, R. M.; Das, S. *Polym. Chem.* **2013**, *4*, 623−628.
(19) Sun, T. L.; Kurokawa, T.; Kuroda, S.; Bin Ihsan, A.; Akasaki, T.; Sato, K.; Haque, M. A.; Nakajima, T.; Gong, J. P. *Nat. Mater.* **2013**, *12*, 932−937.
(20) (a) Sunamoto, J.; Iwamoto, K.; Mohri, Y.; Kominato, T. *J. Am. Chem. Soc.* **1982**, *104*, 5502−5504. (b) Ipe, B. I.; Mahima, S.; Thomas, K. G. *J. Am. Chem. Soc.* **2003**, *125*, 7174−7175. (c) Shao, N.; Jin, J. Y.; Wang, H.; Zheng, J.; Yang, R. H.; Chan, W. H.; Abliz, Z. *J. Am. Chem. Soc.* **2010**, *132*, 725−736.
(21) Achilleos, D. S.; Hatton, T. A.; Vamvakaki, M. *J. Am. Chem. Soc.* **2012**, *134*, 5726−5729.
(22) (a) Goldburt, E.; Shvartsman, F.; Fishman, S.; Krongauz, V. *Macromolecules* **1984**, *17*, 1225−1230. (b) Goldburt, E.; Krongauz, V. *Macromolecules* **1986**, *19*, 246−247.
(23) Mistlberger, G.; Crespo, G. A.; Xie, X. J.; Bakker, E. *Chem. Commun.* **2012**, *48*, 5662−5664.
(24) Casey, J. R.; Grinstein, S.; Orlowski, J. *Nat. Rev. Mol. Cell Biol.* **2010**, *11*, 50−61.
(25) Zhang, L. L.; Huang, J. W.; Si, T.; Xu, R. X. *Expert Rev. Med. Devices* **2012**, *9*, 595−612.
(26) (a) Karton-Lifshin, N.; Albertazzi, L.; Bendikov, M.; Baran, P. S.; Shabat, D. *J. Am. Chem. Soc.* **2012**, *134*, 20412−20420. (b) Redy-Keisar, O.; Kisin-Finfer, E.; Ferber, S.; Satchi-Fainaro, R.; Shabat, D. *Nat. Protoc.* **2014**, *9*, 27−36.

DOI: 10.1021/jacs.5b10127
J. Am. Chem. Soc. 2015, 137, 15262−15275